Appl. Magn. Reson. 8, 475–488 (1995)

Applied Magnetic Resonance

Application of ^{129}Xe NMR Spectroscopy and EXAFS to Probe the Formation of a Bimetallic Cluster in Zeolite Y

C. Pak and R. Ryoo

Department of Chemistry and Center for Molecular Science, Korea Advanced Institute of Science and Technology, Taeduk Science Town, Taejon, Korea

Received September 14, 1994; revised December 20, 1994

Abstract. Palladium was supported on CaY zeolite by ion exchange of $Pd(NH_3)_4^{2+}$ into CaY zeolite, calcination in O_2 and subsequent reduction with H_2. Platinum and silver were added to this Pd/CaY zeolite by ion exchange of $Pt(NH_3)_4^{2+}$ and Ag^+, respectively, and subsequent reduction with Hg. Extended X-ray absorption fine structure of these metals indicates that the successive metal-loading treatments lead first to the formation of a 1-nm Pd cluster inside the supercage of CaY zeolite and to the subsequent formation of bimetallic clusters through incorporation of Pt and Ag atoms into the small Pd cluster. The line width and chemical shift of ^{129}Xe NMR spectrum of xenon gas adsorbed on the zeolite show dramatic changes during the metal clustering procedure, which indicates that ^{129}Xe NMR spectroscopy can be used to probe the formation of bimetallic clusters.

1. Introduction

The zeolites are a group of crystalline, aluminosilicate molecular sieve materials containing a regular array of uniform micropores ranging 0.3–1.3 nm [1]. The zeolite pores are interconnected, forming one, two or three dimensional channels. The zeolite pores are well known as hosts for small metal clusters. Various kinds of metal cluster can be prepared inside zeolite cages via ion exchange or vapor phase deposition of metal species [2]. The metal clusters in zeolite have attracted much attention due to very small size and high catalytic activity for many industrially important chemical reactions such as the conversion of hydrocarbons, NO_x reduction, CO conversion, etc. Perhaps, the most important factor affecting these applications is the cluster size and location in the zeolite [2, 3]. When two metals are supported on a zeolite simultaneously or successively, the question regarding incorporation of the two elements within the same cluster becomes further complicated.

There are reports of a substantial amount of work using ^{129}Xe NMR spectroscopy of adsorbed xenon gas for the investigation of monometallic clusters supported on zeolite [4–15]. The previous studies show that the chemical shift and line width of the ^{129}Xe NMR spectrum are very sensitive to the location and size of metal clusters. These studies indicate that if the metal is well dispersed into small clusters in the zeolite cages, more xenon can be adsorbed on the metal surface than if the metal forms large agglomerates inside or at the external surface of zeolite crystals. This leads to a higher chemical shift for xenon in the well dispersed sample.

There have also been a few other ^{129}Xe NMR studies which indicate that the chemical shift of xenon can be very sensitive to the atomic mixing state in bimetallic zeolite samples [16–18]. In previous ^{129}Xe NMR studies on Pt-Cu and Pt-Ag bimetallic clusters supported on NaY zeolite, the chemical shift decreased as Cu and Ag were added to NaY zeolite containing Pt clusters [16, 17]. When Pt and Ir were simultaneously supported on NaY zeolite, the chemical shift also decreased from the value for a physical mixture of two monometallic zeolites [18]. Thus, the ^{129}Xe NMR studies indicate a negative effect of bimetallic cluster formation on the polarization of xenon at the cluster surface. However, these previous studies on bimetallic zeolite have been performed for immiscible systems in which one metal can screen metal-xenon interactions at the surface of the other cluster, or the structure of the bimetallic cluster has not been confirmed using extended X-ray absorption fine structure (EXAFS) or similar structural analyses.

The present work was performed using ^{129}Xe NMR spectroscopy of a completely miscible Pt-Pd bimetallic system supported on CaY zeolite. The formation of bimetallic clusters was confirmed using EXAFS. The work includes an Ag-Pd system supported on CaY zeolite to obtain more reliable conclusions regarding the applicability of ^{129}Xe NMR for the investigation of bimetallic clusters in zeolites. We also applied a recently developed experimental technique for ^{129}Xe NMR using octamethylcyclotetrasiloxane (OMTS) [19]. This technique has been used to block rapid exchange of xenon gas between adjacent zeolite crystals and thereby to identify the chemical shift of xenon coming from xenon-metal interactions within the zeolite crystal, excluding that from the external surface.

2. Experimental

2.1. Sample Preparation

High purity NaY zeolite was obtained by hydrothermal synthesis using NaOH, sodium aluminate and Ludox HS 40 (Du Pont, 40 wt% SiO_2 and 60 wt% H_2O) [20]. Both the chemical analysis and peak intensity ratios in ^{29}Si NMR of the zeolite gave 2.4 Si/Al to within ± 0.1. The zeolite was ion exchanged with

Ca^{2+} overnight at room temperature (RT) three times repeatedly using an aqueous solution of $CaCl_2$ that contained 2.5 times the quantity of Ca^{2+} required for 100 % ion exchange. This Ca^{2+} ion exchange was performed in order to obtain small Pd cluster size through the $Ca^{2+}\cdots Pd$ interaction in the supercage [11].

$Pt(NH_3)_4^{2+}$ and $Pd(NH_3)_4^{2+}$ were ion exchanged into the CaY zeolites by stirring in aqueous solutions of $Pt(NH_3)_4(NO_3)_2$ (Aldrich) and $Pd(NH_3)_4(NO_3)_2$ (Alpha), respectively, overnight at RT as described previously [11, 12]. The samples were washed with doubly distilled water and dried in a vacuum oven at RT. These samples were placed in a Pyrex U-tube flow reactor, where the ion exchanged Pt and Pd species in zeolite were activated by calcination with flowing O_2 (1 L $min^{-1}g^{-1}$). The calcination temperatures for Pt and Pd were increased from RT to 573 K over 15 h and 623 K over 10 h, respectively, and maintained there for 2 h. The Pt and Pd species in the zeolite were subsequently reduced with flowing H_2 (200 mL $min^{-1}g^{-1}$). The reduction temperatures for Pd and Pt were linearly increased to 673 and 573 K over 20 and 4 h, respectively. The samples were then evacuated at 673 K for 2 h in order to remove chemisorbed hydrogen from the metal clusters. The resulting samples should contain $2H^+$ per reduced metal atom to balance the charge [17]. The samples are designated as $Pd_{7.1}$/CaY and $Pt_{7.1}$/CaY, respectively. The subscript 7.1 represents a nominal number of the metal atoms per unit cell of zeolite, assuming 100 % ion exchange of $Pd(NH_3)_4^{2+}$ and $Pt(NH_3)_4^{2+}$. Chemical analyses for the metals were not performed, but nevertheless the true metal content should not be very different from the nominal loading [11, 12].

The $Pd_{7.1}$/CaY sample was ion exchanged with $Pt(NH_3)_4^{2+}$ overnight at RT using aqueous solutions containing known quantities of $Pt(NH_3)_4(NO_3)_2$. The nominal loadings of Pt were 1.4, 3.5 and 7.1 $Pt(NH_3)_4^{2+}$ per unit cell of zeolite. The samples after the ion exchange were washed with distilled water and dried in a vacuum oven at RT. These samples were then reduced with flowing H, while the temperature was linearly increased from RT to 573 K over 4 h and maintained for 2 h. The samples were then evacuated for 2 h at 673 K. These treatments gave a series of $Pt_xPd_{7.1}$/CaY samples with x equal to 1.4, 3.5 and 7.1.

Similar treatments of the $Pd_{7.1}$/CaY sample using ion exchange of Ag^+ and subsequent reduction at 673 K gave a series of $Ag_xPd_{7.1}$/CaY samples with x equal to 1.4, 3.5 and 7.1. All other experimental conditions for the preparation of $Ag_xPd_{7.1}$/CaY were identical to those used for $Pt_xPd_{7.1}$/CaY.

2.2. ^{129}Xe NMR

The Pyrex U-tube flow reactor used for sample preparation was joined with an NMR tube that was equipped with a homemade vertical ground-glass vacuum stopcock as shown in Fig. 1. The bimetallic samples after preparation were transferred into the NMR tube by tilting the reactor. The sample, placed in the NMR

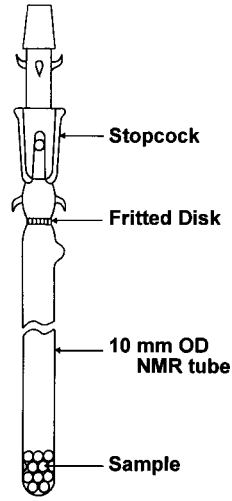

Fig. 1. Detailed description of NMR tube used for the ^{129}Xe NMR experiment.

tube under vacuum, were then sealed by flame [19]. Monometallic $Pt_{7.1}/CaY$ and $Pd_{7.1}/CaY$ samples exposed to air after preparation were reduced again with flowing H_2 for 1 h at 573 K, evacuated for 1 h at 673 K and transferred to NMR tubes, using the same reactor.

Natural xenon gas (Matheson, 99.995 %) was equilibrated with the sample in the NMR tube, over 30 min to a given pressure ranging 6.7 to 53.3 kPa at 296 K. ^{129}Xe NMR spectra were obtained at 296 K with a Bruker AM 300 instrument operating at 83.0 MHz for ^{129}Xe with a 0.5-s relaxation delay. Data acquisition time for each NMR spectrum was dependent on the NMR line width and the xenon pressure, taking from 10 min to several hours. The chemical shift was referenced to xenon gas extrapolated to zero pressure.

2.3. EXAFS

150–200 mg of powdered sample, that was exposed to air after preparation, was pressed into a self-supporting wafer, 10 mm in diameter. The sample wafer was reduced again in flowing H_2 at 573 K, using a Pyrex U-tube flow reactor that was joined with an EXAFS cell in a similar manner to that used for the ^{129}Xe NMR tube. The EXAFS cell had Kapton (Du Pont, 125 μm thick) windows which were attached using Torr Seal (Varian). After the sample was transferred into the EXAFS cell, the sample in the cell under a H_2 atmosphere was sealed off by flame. EXAFS was measured in a transmission mode at Pt L_{III} and Pd L_{III} edges at RT by using beamline 10 B at the Photon Factory of the National Laboratory for High Energy Physics (KEK-PF) in Tsukuba, Japan. A Si(311)

channel cut monochromator was used. The resolution ($\Delta E/E$) was $1.0 \cdot 10^{-4}$ at the Pt L_{III} edge and $2.5 \cdot 10^{-4}$ at the Pd K edge. The X-ray energy for the Pt and Pd EXAFS was increased in 2.2 and 2.5 eV steps, respectively. The X-ray intensity was measured using gas ionization chambers. Analysis of the X-ray absorption data was carried out by standard methods using the UWXAFS2 program package distributed by the University of Washington [21].

3. Results and Discussion

3.1. Pt-Pd Bimetallic Clusters Probed by EXAFS

EXAFS oscillations for $Pt_xPd_{7.1}$/CaY shown in Fig. 2 have been obtained by multiplication of the wave vector cubed after removing the background and normalizing the X-ray absorption spectra above the absorption edges. Fourier transformation of the EXAFS oscillations has been performed from $23 \leq k \leq 125$ nm^{-1} to $0 \leq R \leq 1.00$ nm for Pt EXAFS and from $25 \leq k \leq 135$ nm^{-1} to $0 \leq R \leq 1.00$ nm for Pd EXAFS. The Fourier transforms thus obtained are presented in Fig. 3. Intense peaks corresponding to metal-metal first shell appear from 0.15 to 0.31 nm (before phase shift correction) in the Fourier transforms while a weaker peak 5.8 around 0.21 nm comes from a nonlinear k-dependence of the phase shift and low-frequency variation in the backscattering amplitude function [22]. The first-shell peak around the Pd atom in Fig. 3a shifts continuously from 0.255 to 0.261 nm as more Pt is added to $Pd_{7.1}$/CaY. Simultaneously, the position of the first shell peak around the Pt atom (see Fig. 3b) increases from 0.249 to 0.276 nm. These changes in EXAFS with the addition of Pt are a qualitative indication of

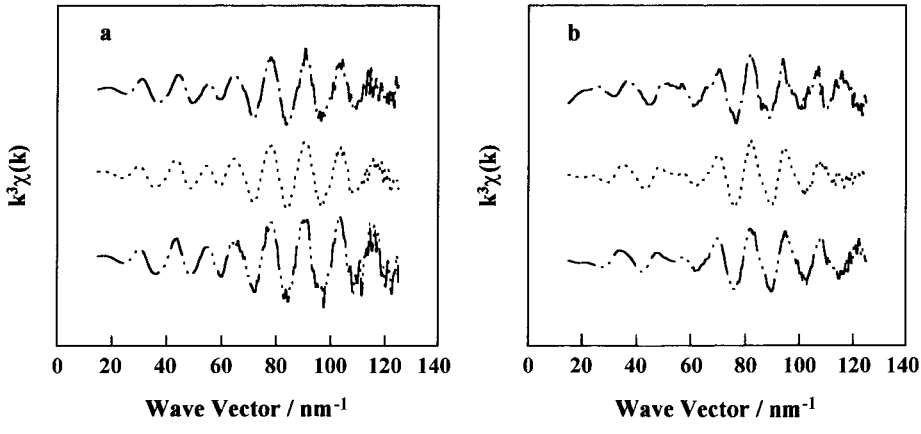

Fig. 2. k^3-weighted EXAFS oscillations obtained from (**a**) Pd K and (**b**) Pt L_{III} edges of (– · · –) $Pt_{1.4}Pd_{7.1}$/CaY, (· · ·) $Pt_{3.5}Pd_{7.1}$/CaY and (– · –) $Pt_{7.1}Pd_{7.1}$/CaY.

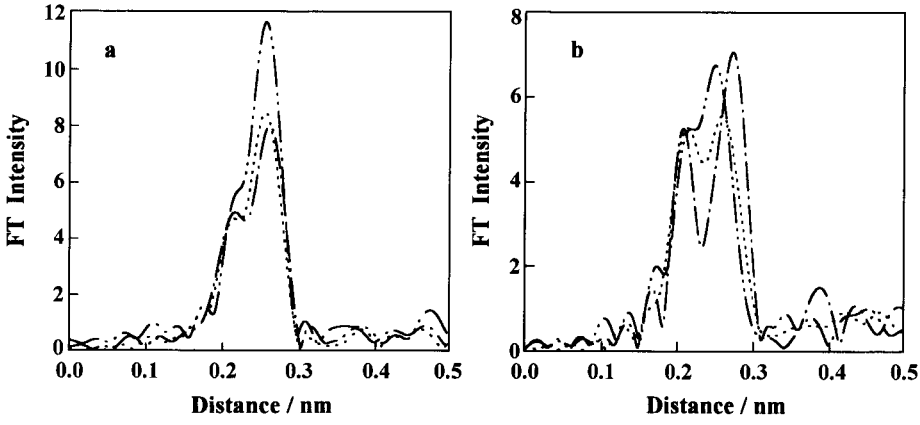

Fig. 3. Fourier transforms of k^3-weighted EXAFS spectra at (**a**) Pd K and (**b**) Pt Lm edges of (– · · –) $Pt_{1.4}Pd_{7.1}$/CaY, (· · ·) $Pt_{3.5}Pd_{7.1}$/CaY and (– · –) $Pt_{7.1}Pd_{7.1}$/CaY.

the formation of Pt-Pd bimetallic clusters via the incorporation of Pt atoms to Pd clusters in $Pd_{7.1}$/CaY.

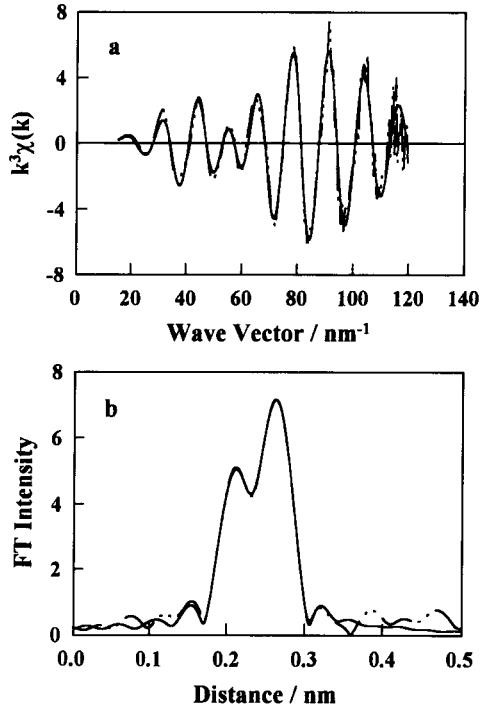

Fig. 4. (**a**) EXAFS spectra and (**b**) the Fourier transforms obtained from $Pt_{7.1}Pd_{7.1}$/CaY at Pd K edge; (– · · –) experimental and (–) theoretical fit using UWXAFS2 and FEFF5 codes.

To obtain the structural parameters, curve fitting of both the Fourier transform in R-space and the EXAFS oscillation in k-space was performed simultaneously by using reference spectra which were obtained theoretically for all atomic pairs, i.e., Pd-Pd, Pd-Pt, Pt-Pd and Pt-Pt, with the amplitude reduction factor (S_0^2) equal to 0.90 for Pd absorber and 0.89 for Pt absorber, respectively, by using automated codes UWXAFS2 and FEFF5 [23]. Results of the EXAFS curve fitting for $Pt_{7.1}Pd_{7.1}$/CaY at the Pd K edge are shown in Fig. 4. The structural parameters are listed in Table 1.

In Table 1, the coordination number $N_{M\text{-}M'}$ is defined as the number of the nearest neighbor atoms M′ around atom M. N_M is the sum for all neighbor metal atoms around M. N_{total} is an average metal coordination number defined for the metal cluster as $N_{Pd}W_{Pd} + N_{Pt}W_{Pt}$, where W_M is the atomic percentage of M in the total metal. The coordination numbers in Table 1 satisfy the condition for equal coordination between Pt-Pd and Pd-Pt, that is, $N_{Pt\text{-}Pd}W_{Pt} = N_{Pd\text{-}Pt}W_{Pd}$ within a permissible curve fitting error limit. The nearest neighbor distances also satisfy $R_{Pt\text{-}Pd} = R_{Pd\text{-}Pt}$ (=0.274 nm) to within ±0.001 nm. The formation of Pt-Pd bimetallic clusters is indicated by Pt-Pd coordination numbers that are significantly different from zero. Significant increases in the cluster size can be considered with the Pt addition to $Pd_{7.1}$/CaY, since N_{total} increases from 7.7 to 8.6 as the Pt loading increases up to 7.1 Pt per unit cell of zeolite. $N_{Pd\text{-}Pt}$ also increases from 1.1 to 3.3 as the Pt loading increases from 1.4 to 7.1 Pt per unit

Table 1. Structural parameters for $Pt_xPd_{7.1}$/CaY obtained from curve fitting of EXAFS data at Pd K and Pt L_{III} edges.

Sample	Atomic pair	R[a] (nm)	N[b]	N_{total}[c]
$Pd_{7.1}$/CaY	Pd-Pd	0.281	7.3	
$Pt_{1.4}Pd_{7.1}$/CaY	Pd-Pd	0.278	6.8	7.7
	Pd-Pt	0.275	1.1	
	Pt-Pd	0.273	4.2	
	Pt-Pt	0.272	2.7	
$Pt_{3.5}Pd_{7.1}$/CaY	Pd-Pd	0.277	5.6	8.1
	Pd-Pt	0.274	2.4	
	Pt-Pd	0.275	3.5	
	Pt-Pt	0.272	4.8	
$Pt_{7.1}Pt_{7.1}$/CaY	Pd-Pd	0.276	4.6	8.6
	Pd-Pt	0,274	3.3	
	Pt-Pd	0.274	3.4	
	Pt-Pt	0.274	5.8	
$Pt_{7.1}$/CaY	Pt-Pt	0.274	6.2	

[a] Nearest neighbor distance with ±0.001 nm.

[b] Nearest neighbor coordination number with ±1.0.

[c] $N_{total} = N_{Pd}W_{Pd} + N_{Pt}W_{Pt}$, where N_M is coordination number around M metal and W_M is atomic percentage of M metal.

cell. These changes in the coordination numbers indicate that bimetallic clusters are formed through the incorporation of Pt atoms into Pd clusters in CaY.

3.2. Chemical Shift in the ^{129}Xe NMR Spectrum for Metal Clusters in Zeolite

Typical ^{129}Xe NMR spectra of CaY, $Pt_{7.1}$/CaY, $Pd_{7.1}$/CaY and $Pt_xPd_{7.1}$/CaY are presented in Fig. 5. A single Lorentzian line was observed in each spectrum. Such a single Lorentzian line shape indicates that the metal-containing zeolite samples are homogeneous from the viewpoint of a xenon diffusion distance on the NMR time scale. Previous studies using ^{129}Xe NMR of zeolite mixtures have shown coalescence of two NMR lines when Y zeolites containing different met-

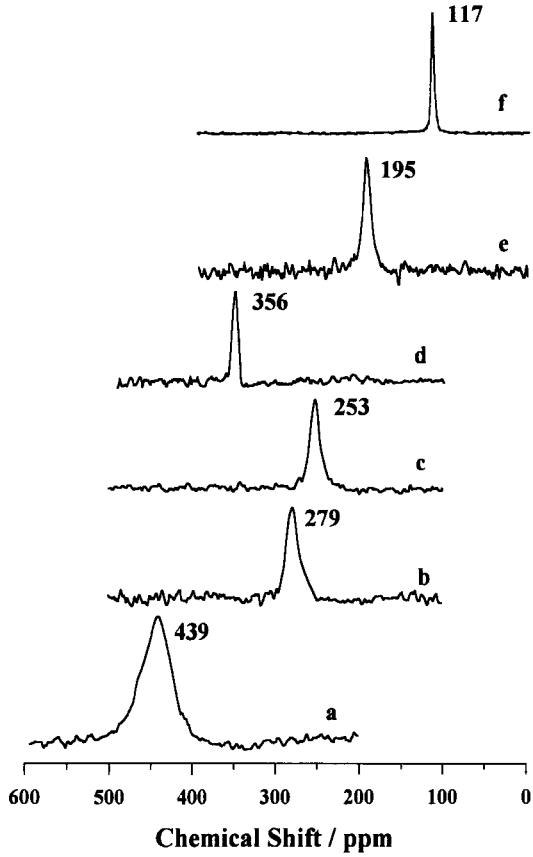

Fig. 5. ^{129}Xe NMR spectra of xenon adsorbed on (**a**) $Pd_{7.1}$/CaY, (**b**) $Pt_{1.4}Pd_{7.1}$/CaY, (**c**) $Pt_{3.5}Pd_{7.1}$/CaY, (**d**) $Pt_{7.1}Pd_{7.1}$/CaY, (**e**) $Pt_{7.1}$/CaY and (**f**) CaY. All the spectra were measured at 296 K and 53.3 kPa.

al clusters or cations are well mixed, confirming rapid xenon exchange between Y-zeolite crystals of approximately 1 μm size [8, 24]. The broad ^{129}Xe NMR line width is probably due to xenon adsorption on metal clusters with large paramagnetic moment. Other studies using transmission electron microscopy, EXAFS, wide angle X-ray scattering and xenon adsorption isotherms confirm that the size of Pt and Pd clusters prepared in CaY zeolite, following the same procedures used in the present work, is about 1 nm [7, 11, 12]. These clusters are randomly located in the zeolite supercages.

The Pd-Pd coordination number given for $Pd_{7.1}$/CaY in Table 1 agrees approximately with a 1-nm Pd cluster. Assuming that a Pd cluster of 50–60 Pd atoms is located inside the supercage [11], it follows that one supercage out of every 60–70 supercages is believed to contain a cluster. A single Lorentzian NMR line is obtained due to rapid xenon exchange between the metal cluster and the empty supercages.

In Fig. 6, the chemical shift for metal-containing samples decreases monotonically while the chemical shift for CaY zeolite shows a shallow minimum around 26.7 kPa. Recently, the chemical shift decrease with pressure has been explained by a rapid xenon exchange between strong adsorption sites and weak sites [6, 12, 25–27]. It is believed that metal clusters and multivalent cations located inside the supercages are the strong adsorption sites while monovalent cations and

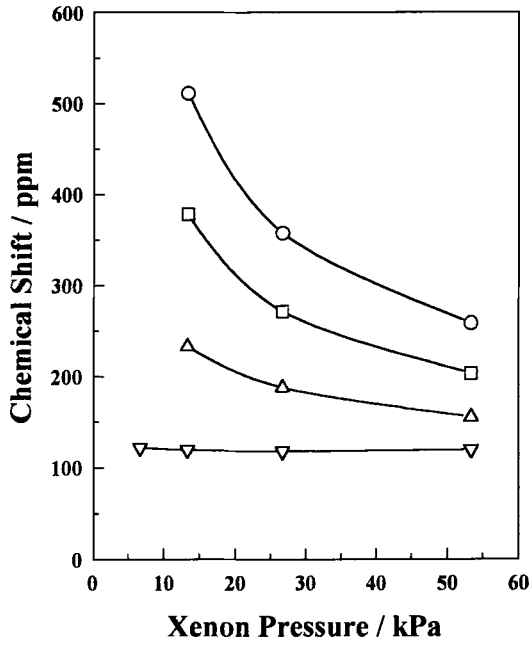

Fig. 6. The chemical shift of ^{129}Xe from xenon adsorbed on (○) $Ag_{1.4}Pd_{7.1}$/CaY, (□) $Ag_{3.5}Pd_{7.1}$/CaY, (△) $Ag_{7.1}Pd_{7.1}$/CaY and (▽) CaY plotted against the xenon pressure.

the aluminosilicate framework surface in zeolite are the weak adsorption sites. However, metal clusters or multivalent cations located inside the sodalite cage are not believed to cause significantly large chemical shifts since the diameter of xenon (0.44 nm) is too large to enter through a sodalite cage aperture (0.22 nm).

At very low pressures, xenon adsorption is believed to occur selectively at the strong adsorption sites. The interaction of the xenon with these sites leads to strong polarization and consequently the chemical shift increases. The number of strong sites is very small compared with the number of weak adsorption sites which occupy most of the zeolite surface. Thus, strong adsorption sites become saturated with xenon while the population of adsorbed xenon on weak adsorption sites increases in a linear fashion with increasing xenon pressure [11–13]. Averaging of the chemical shift due to rapid exchange of xenon between strong and weak adsorption sites is weighted progressively more towards the weak adsorption sites as the pressure is increased. This leads to a negative slope at low pressure in the chemical shift-vs.-pressure curve, For very high pressures the xenon-xenon interaction term becomes important and therefore the chemical shift increases. Following a two-site exchange model used previously [11, 27], the chemical shift δ can then be written as:

$$\delta \simeq \delta_{\text{S-Xe}} + \delta_{\text{Xe-Xe}} = f_{\text{S}}\delta_{\text{SS-Xe}} + f_{\text{W}}\delta_{\text{WS-Xe}} + \delta_{\text{Xe-Xe}} , \qquad (1)$$

where $\delta_{\text{S-Xe}}$ is the chemical shift component due to interaction of Xe with the surface, $\delta_{\text{Xe-Xe}}$ is the component due to the xenon-xenon interaction, $\delta_{\text{SS-Xe}}$ is the component of the chemical shift for the interaction of xenon with a strong adsorption site, $\delta_{\text{WS-Xe}}$ is the component due to interaction with a weak adsorption site, f_{S} can be defined as the mole fraction of adsorbed xenon in the strong adsorption site, f_{W} is the mole fraction in the weak adsorption site, and it should be noted that $f_{\text{S}} + f_{\text{W}} = 1$.

3.3. Chemical Shift Change in the ^{129}Xe NMR Spectrum due to Formation of Bimetallic Clusters

In Fig. 5, effects of the addition of Pt to $Pd_{7.1}$/CaY are shown by the ^{129}Xe NMR spectra obtained at the same temperature and pressure. The chemical shift obtained at 53.3 kPa and 296 K decreased from 439 to 279 ppm as 1.4 Pt per unit cell of zeolite was added to $Pd_{7.1}$/CaY. The chemical shift showed a further decrease to 253 ppm as 3.5 Pt per unit cell was added to $Pd_{7.1}$/CaY. Three cases may be considered when Pt is reduced after ion exchange of $Pt(NH_3)_4^{2+}$ into $Pd_{7.1}$/CaY.

Firstly, a small Pt cluster may be obtained through agglomeration of the Pt atoms into an empty supercage. In this case, Pd and Pt will not form a bimetallic cluster. The formation of a new Pt cluster will lead to an increase in the chemical shift.

Secondly, the Pt atoms may migrate to adjacent supercages within the zeolite crystal or on the external surface of zeolite to form large Pt clusters. Bimetallic clusters are not formed. In this case, the total surface area of the large Pt particles will be much smaller than that of the small Pt clusters considered in the first case. As a result, the chemical shift increase due to Pt addition will be much smaller than in the case of small Pt clusters.

Finally, a situation can be considered in which the Pt atoms are incorporated into 1-nm Pd clusters, forming small bimetallic Pt-Pd clusters. In this case, the chemical shift may increase or decrease depending on the magnitude of the polarization of xenon adsorbed on the bimetallic clusters. If the chemical shift is observed to increase, it is difficult to distinguish between this and the first case. If the chemical shift decreases as shown in Fig. 7, the chemical shift change may be used as a necessary condition for the formation of bimetallic clusters. However, changes in the chemical shift can be the result of sample contamination. The ^{129}Xe NMR spectroscopic technique is very convenient for detecting a difference between samples, but the cause of the chemical shift difference should be further characterized using EXAFS or other similar structural analyses.

Since the coordination numbers obtained from EXAFS of $Pt_{7.1}Pd_{7.1}$/CaY satisfy $N_{Pt\text{-}Pt}/W_{Pt} \gg N_{Pt\text{-}Pd}/W_{Pd}$, it is considered that the Pt atoms are not mixed uniformly with Pd. Some of the Pt atoms seem to be mixed with the small Pd clusters,

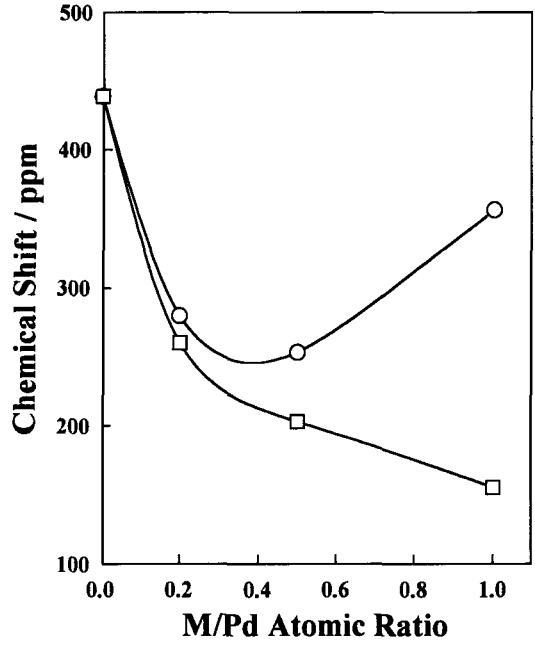

Fig. 7. The chemical shift of ^{129}Xe from xenon adsorbed on (○) $Pt_xPd_{7.1}$/CaY and (□) $Ag_xPd_{7.1}$/CaY samples plotted against the M/Pd atomic ratio.

while others agglomerate to form large Pt clusters. As shown in Fig. 7, the chemical shift of $Pt_{7.1}Pd_{7.1}$/CaY (356 ppm) is larger than that of $Pt_{3.5}Pd_{7.1}$/CaY (253 ppm). This conforms to a combination of the first and the third cases, as described above.

In Fig. 7, the ^{129}Xe NMR chemical shift of $Ag_xPd_{7.1}$/CaY obtained at 53.3 kPa and 296 K is plotted against the Ag/Pd atomic ratio. The chemical shift decreased from 439 ppm to 258, 203 and 155 ppm successively as the Ag loadings in $Pd_{7.1}$/CaY increased to 1.4, 3.5 and 7.1 atoms per unit cell of zeolite. The decreases in the chemical shift due to successive loading of metals on zeolite have also been found with CuPt/NaY and AgPt/NaY in previous studies [16, 17]. These results correspond to a mechanism for the formation of bimetallic clusters through the addition of one metal to clusters of another metal located in the supercages of Y zeolite. However, the second metal added can form a separate phase under high loading as has been seen for $Pt_{7.1}Pd_{7.1}$/CaY. The degree to which a separate phase forms seems to depend on a particular bimetallic system and also on the cluster size.

3.4. Probing Inside of Zeolite Crystals by ^{129}Xe NMR

Recently, Ryoo *et al.* [19] have suggested a ^{129}Xe NMR spectroscopic technique: surrounding zeolite crystals with OMTS in order to block the intercrystalline diffusion of xenon. They have demonstrated that both Pt/NaY and Ni/NaY can show much larger chemical shifts than NaY zeolite, both for Ni clusters located on the external surface of the zeolite crystal and Pt clusters located inside the supercages. When OMTS was used to surround the crystal surface, the Pt/NaY still maintained a very high chemical shift due to the presence of the clusters inside the supercages. In contrast, the chemical shift for Ni/NaY decreased to a value similar to that for NaY. The xenon was entrapped inside the zeolite crystal by OMTS, and thus the interaction of xenon with Ni clusters located at the external surface of zeolite crystals was blocked by OMTS.

Figure 8 shows ^{129}Xe NMR spectra obtained for $Pt_{1.4}Pd_{7.1}$/CaY before and after surrounding the zeolite crystals with OMTS. The $Pt_{1.4}Pd_{7.1}$/CaY sample was reduced at 573 K with H_2 and evacuated at 673 K in an NMR cell that was joined to another tube containing liquid OMTS. The sample was equilibrated with 53.3 kPa xenon gas at 296 K. The NMR tube containing the zeolite sample was flame-sealed after the sample was soaked with OMTS in the presence of xenon as described previously [19]. The ^{129}Xe NMR spectrum, showing a broad signal at 256 ppm in Fig. 8a, was obtained before the addition of OMTS. The ^{129}Xe NMR spectra presented in Figs. 8b and 8c were obtained approximately 2 and 10 h, respectively, after the addition of OMTS.

The addition of OMTS to $Pt_{1.4}Pd_{7.1}$/CaY resulted in the appearance of two NMR signals. One narrow line at 187 ppm was due to the xenon gas dissolved in the

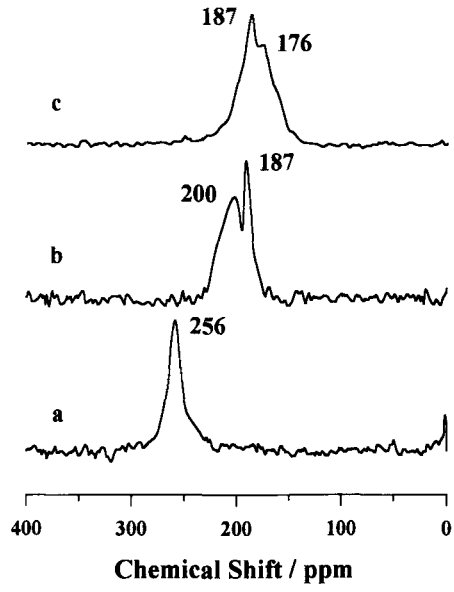

Fig. 8. ^{129}Xe NMR spectra of xenon adsorbed on (**a**) $Pt_{1.4}Pd_{7.1}$/CaY, (**b**) $Pt_{1.4}Pd_{7.1}$/CaY 2 h and (**c**) 10 h after the addition of OMTS.

OMTS phase [19]. The other broad line (centered at 200 ppm in Fig. 8b and 176 ppm in Fig. 8c) came from the xenon which was entrapped inside the zeolite by the OMTS layer on the crystal surface. Thus, the chemical shift of xenon inside the zeolite crystal decreased gradually with time after the addition of OMTS. This chemical shift change with time may be attributed to a pressure increase inside the zeolite crystal due to slow diffusion of the OMTS layer towards the center of the zeolite crystal [19]. The chemical shift value extrapolated to time zero was around 250 ppm. Such a chemical shift which is much greater than the value for CaY zeolite provides strong evidence that the metal clusters are located inside the zeolite crystal.

4. Conclusion

In the present work, the chemical shift in the ^{129}Xe NMR spectrum of zeolite decreases as Pt and Ag are incorporated into CaY zeolite containing 1-nm Pd clusters by the reduction of Pt and Ag species after ion exchange of $Pt(NH_3)_4^{2+}$ and Ag^+ into the Pd/CaY. This chemical shift change corresponds to the formation of bimetallic clusters through incorporation of Pt or Ag atoms in the 1-nm Pd clusters, as confirmed by EXAFS. However, it is difficult to draw general conclusions on the chemical shift decrease as a function of the formation of bimetallic clusters. The chemical shift may increase for other cases of bimetallic clus-

ter formation, or the chemical shift may decrease due to sample contamination occurring during introduction of the second metal. ^{129}Xe NMR can be very conveniently used for detecting any difference between samples. However, structural differences should be clarified using other structural analysis techniques.

Acknowledgements

This work was supported from the Korea Science and Engineering Foundation. The EXAFS experiment was supported by Photon Factory (Proposal No. 92-G193) and Pohang Accelerator Laboratory.

References

[1] Bhatia B.: Zeolite Catalysts: Principles and Applications. Boca Raton: CRC Press, Inc. 1990.
[2] Sachtler W.M.H., Zhang Z.: Adv. Catal. **39**, 129–220 (1993)
[3] Che M., Bennett C.O.: Adv. Catal. **36**, 55–171 (1989)
[4] Ito T., de Menorval L.-C., Fraissard J.P.: J. Chim. Phys. **80**, 573–578 (1983)
[5] Primet M., de Menorval L.-C., Fraissard J.: J. Chem. Soc., Faraday Trans. I **81**, 2867–2874 (1985)
[6] Scharpf E.W., Crecely R.W., Gates B.C., Dybowski C.: J. Phys. Chem. **90**, 9–11 (1986)
[7] Boudart M., Samant M.G., Ryoo R.: Ultramicroscopy **20**, 125–134 (1986)
[8] Shoemaker R., Apple T.: J. Phys. Chem. **91**, 4024–4029 (1987)
[9] Chmelka B.F., Ryoo R., Liu S.-B., de Menorval L.-C., Radke C.J., Petersen E.E., Pines A.: J. Am. Chem. Soc. **110**, 4465–4467 (1988)
[10] Coddington J.M., Howe R.F., Yong Y.-S., Asakura K., Iwasawa Y.: J. Chem. Soc. Faraday Trans. **86**, 1015–1016 (1990)
[11] Kim J.-G., Ihm S.-K., Lee J.Y., Ryoo R.: J. Phys. Chem. **95**, 8546–8552 (1991)
[12] Ryoo R., Cho S. J., Pak C., Kim J.-G., Ihm S.-K., Lee J. Y.: J. Am. Chem. Soc. **114**, 76–82 (1992)
[13] Cho S.J., Jung S.M., Shul Y.G., Ryoo R.: J. Phys. Chem. **96**, 9922–9927 (1992)
[14] Trescos E., de Menorval L.-C., Rachdi F.: J. Phys. Chem. **97**, 6943–6944 (1993)
[15] Pak C., Cho S,J., Lee J.Y., Ryoo R.: J. Catal. **149**, 61–69 (1994)
[16] Ahn D. H., Lee J.S., Nomura M., Sachtler W.M.H., Moretti G., Woo S.I., Ryoo R.: J. Catal. **133**, 191–201 (1992)
[17] Ryoo R., Pak C., Cho S.J.: Jpn. J. Appl. Phys. **32**, S.32–2, 475–477 (1993)
[18] Yang O.B., Woo S.I., Ryoo R.: J. Catal. **137**, 357–367 (1992)
[19] Ryoo R., Kwak J.H., de Menorval L.-C.: J. Phys. Chem. **98**, 7101–7103 (1994)
[20] Rollmann L.D., Valyosik E.W.: Inorp. Syn. **22**, 61–68 (1983)
[21] Newville M., Livins P., Yacoby Y., Rehr J.J., Stern E.A.: Phys. Rev. B **47**, 14126–14131 (1993)
[22] Prins R., Koningsberger D.C. in: X-ray Absorption: Principles, Applications, Techniques of EXAFS, SEXAFS and XANES (Koningsberger D.C., Prins R., eds.), pp. 321–372. New York: John Wiley & Sons 1988.
[23] Rehr J.J., Albers R.C., Zabinsky S.I.: Phys. Rev. Lett. **69**, 3397–3400 (1992)
[24] Ryoo R., Pak C., Chmelka B.F.: Zeolites **10**, 790–793 (1990)
[25] Ito T., Fraissard J.: J. Chem. Soc. Faraday Trans. I **83**, 451–462 (1987)
[26] Pak C., Ryoo R.: J. Korean Chem. Soc. **36**, 351–359 (1992)
[27] Kim J.-G., Kompany T., Ryoo R., Ito T., Fraissard J.: Zeolites **14**, 427–432 (1994)

Author's address: Prof. Dr. Ryong Ryoo, Department of Chemistry and Center for Molecular Science, Korea Advanced Institute of Science and Technology, Taeduk Science Town, Taejon 305-701, Korea